A Mass Budget Analysis on the Interannual Variability of the Polar Surface Pressure in the Winter Season

YUEYUE YU

LASG, Institute of Atmospheric Physics, Chinese Academy of Sciences, and University of Chinese Academy of Sciences, Beijing, China

RONGCAI REN, JINGGAO HU, AND GUOXIONG WU

LASG, Institute of Atmospheric Physics, Chinese Academy of Sciences, Beijing, China

(Manuscript received 15 November 2013, in final form 29 April 2014)

ABSTRACT

This study reports a mass budget analysis on the year-to-year variability of the winter [December–February (DJF)]-mean Arctic (60°–90°N) surface pressure (Ps) using the 33-yr daily Interim ECMWF Re-Analysis (ERA-Interim; 1979–2011). The analysis reveals that the interannual variability of mass transported into the Arctic region in upper layers plays a dominant role in the interannual variability of the winter-mean Arctic Ps anomalies. When winter-mean Arctic Ps anomalies are positive, both the transport of mass into the Arctic region in the upper layer by the poleward branch of meridional mass circulation and the transport of mass out of the Arctic region in the lower layer by the equatorward branch tend to strengthen and vice versa. In the earlier winter months from November to December, mass anomalies transported in overwhelm those transported out, explaining the mass source of winter-mean Arctic Ps anomalies. The coupling between adiabatic mass transport by meridional mass circulation and diabatic processes explains why, over the Arctic region, yearly variations of winter Ps are positively correlated with mass anomalies in the upper layer (above 290 K) and near the surface (below 260 K) but negatively correlated with mass anomalies in the middle and lower troposphere (between 260 and 290 K). In winters with positive (negative) Arctic Ps anomalies, wave activity, particularly in wavenumbers 1 and 2, is stronger (weaker) in the extratropical stratosphere in the earlier winter months from November to January, coincident with the interannual variability of the meridional mass circulation intensity in winter seasons.

1. Introduction

Climate variability of Arctic surface pressure (Ps) is intimately related to the leading recurrent oscillation modes in the northern extratropics, namely the Arctic Oscillation/North Atlantic Oscillation (AO/NAO) (Kuroda 2005) and the northern annular mode (NAM) (Lorenz 1951; Kodera et al. 1990; Thompson and Wallace 1998; Baldwin and Dunkerton 1999; Baldwin 2001). The positive (negative) phase of AO/NAM is characterized with a decrease (increase) in polar Ps surrounded by an increase (decrease) in Ps along the midlatitude belt. Those leading oscillation modes are closely linked to extreme temperature events, storms, and other anomalous weather or climate phenomena in the extratropics (Balling and Lawson 1982; Thompson and Wallace 1998; Thompson and Wallace 2001; Moritz et al. 2002). Therefore, variations of the Arctic Ps are important indicators of changes in the extratropical large-scale circulation and their related climate anomalies.

When considering changes of Arctic Ps, one would think that mass changes in the troposphere would play a leading role because most of the air mass resides in the troposphere. At intraseasonal time scales, the AO (and thereby polar Ps) is related to the Madden–Julian oscillation (MJO) via modulations of the extratropical atmospheric circulation by MJO-induced anomalous convection activities over the Indian Ocean (Miller et al. 2003; Zhou and Miller 2005; L'Heureux and Higgins 2008). The long-term trend of the AO has been attributed to anthropogenic radiative forcing as evident by a positive trend during 1950–2000 (Walsh et al. 1996;

Corresponding author address: Dr. Rongcai Ren, LASG, Institute of Atmospheric Physics, CAS, P.O. Box 9804, 100029 Beijing, China. E-mail: rrc@lasg.iap.ac.cn

DOI: 10.1175/JAS-D-13-0365.1

Gillett et al. 2002, 2003, 2005), although the positive trend appears to reverse in the last decade (Overland and Wang 2005; L'Heureux et al. 2010). Both observational and modeling studies indicate the important role of stratospheric processes in leading to climate variations of the AO and Arctic Ps. For instance, oscillations of stratospheric polar vortex (Black 2002) and polar night jet (Kuroda and Kodera 2004) are related to the surface circulation anomalies in the extratropics at intraseasonal time scales. A systematic downward propagation of geopotential height and zonal wind anomalies in the polar stratosphere was found during the NAM events (Kodera et al. 1990; Baldwin and Dunkerton 1999; Waugh et al. 1999; Baldwin and Dunkerton 2001; Thompson et al. 2002; Sigmond et al. 2003; Limpasuvan et al. 2004). The observed long-term trend of Arctic Ps (and AO) was only captured in climate models that resolve stratospheric dynamics (Shindell et al. 1999).

One mechanism for the downward propagation of stratospheric anomalies is the interaction between the upward-propagating planetary waves and zonal-mean flow (Charney and Drazin 1961; Matsuno 1970; Hines 1974b; Holton and Mass 1976; Kodera et al. 1996). Another possible mechanism is that the upward-propagating planetary waves that themselves drive the stratosphere can be reflected downward, hence modifying the planetary wave activity in the troposphere (Hines 1974a; Sato 1974; Geller and Alpert 1980; Perlwitz and Harnik 2003). Cai and Ren (2007) and Ren and Cai (2008) found that there exists simultaneous poleward and downward propagation of circulation anomalies of both signs in the stratosphere. The poleward propagation in the upper stratosphere tends to lead that in the lower stratosphere. Such delayed poleward propagation in lower levels implies a downward propagation accompanied with poleward propagation in the stratosphere [see Figs. 2 and 3 in Ren and Cai (2007)]. Cai and Ren (2007) proposed that the simultaneous poleward and downward propagation in the stratosphere and the equatorward propagation in the troposphere are associated with variations of meridional mass circulation. The poleward-propagating positive (negative) stratospheric temperature anomalies are associated with a stronger (weaker) warm-air branch of the meridional mass circulation. The variability of the compensating cold-air branch lags that of the warm-air branch, causing the equatorward-propagating negative (positive) tropospheric temperature anomalies following the arrival of the poleward positive (negative) temperature anomalies in the polar stratosphere. Besides the out-of-phase relationship between the stratospheric and tropospheric temperature anomalies in the polar region, an in-phase relation between mass anomalies in the stratosphere and surface pressure anomalies is also documented. This explains the seemingly "barotropic structure" of geopotential height anomalies of both signs during NAM events, namely, a stratospheric cold low anomaly above a surface warm low anomaly or a stratospheric warm high anomaly above a surface cold high anomaly over the Arctic region.

In this study, we wish to provide a quantitative estimation of contributions of interannual mass changes in the stratosphere and troposphere to the interannual variability of Arctic Ps in the winter season through a quantitative mass budget analysis associated with variability of meridional mass circulation. The primary scientific questions that we attempt to address include the following: What is the relationship between the yearly changes of polar Ps and those of the air mass in each isentropic layer from the troposphere to the stratosphere in winter? How is the mass budget over the polar region modulated by the overturning meridional mass circulation in the troposphere and stratosphere? The answers to these questions would help further advance our understanding of the stratosphere–troposphere coupling as well as its effects on the year-to-year variability of Arctic Ps.

2. Data and methodology

a. Data

The data used in this study include daily surface pressure, temperature, and wind, and three-dimensional wind, temperature, and geopotential height fields from Interim European Centre for Medium-Range Weather Forecasts (ECMWF) Re-Analysis (ERA-Interim) data covering the period from 1 January 1979 to 31 December 2011 (Dee et al. 2011). The data fields are on 1.5° latitude × 1.5° longitude grids and at 37 pressure levels spanning from 1000 to 1 hPa.

The winter means are defined as averages from December to February (DJF). The climatological-mean fields were obtained by averaging the winter-mean data across all years from 1979 to 2011. The year-to-year anomalies in winter seasons are obtained straightforwardly by removing the climatological winter means from the yearly DJF means of total fields. Unless specified otherwise, we below refer them simply as "anomalies" without referencing "in winter." In particular, we refer temporal and area-weighted spatial mean of surface pressure anomalies over the Arctic region (60°–90°N) and in each winter season simply as "polar Ps anomalies." The index of polar Ps anomalies measures the interannual variability of the total air mass above the polar circle in winter seasons.

b. Isentropic mass and mass flux calculation

Following Pauluis et al. (2008, 2010), we have interpolated all the data fields onto 200 equally spaced sigma levels from 1 to 0. The air mass δm_σ in each grid cube between two adjacent sigma surfaces was calculated based on

$$\delta m_\sigma = \mathrm{Ps}\frac{\delta\sigma}{g}, \tag{1}$$

where Ps is in pascals, g is the gravitational acceleration, and $\delta\sigma = 1/200$. We then derived the air mass m between adjacent isentropic surfaces (Θ_n and Θ_{n+1}) in each grid point on daily basis according to

$$m(\lambda,\phi,\Theta_n,t) = \int_0^1 \delta m_\sigma(\lambda,\phi,t)Y[\theta(\lambda,\phi,\sigma,t),\Theta_n,\Theta_{n+1}]\,d\sigma, \tag{2}$$

where $Y(x, x_1, x_2) = 1$ when $(x_1 \le x < x_2)$ and otherwise $Y(x, x_1, x_2) = 0$. In Eq. (2), $\theta(\lambda, \phi, \sigma, t)$ is potential temperature derived from 3D air temperature field; Θ_n is equal to $\theta_{\min}(\lambda, \phi, t)$ or one of the 15 preselected potential temperature surfaces that is above $\theta_{\min}(\lambda, \phi, t)$, whereas Θ_{n+1} is the one of the 15 preselected potential temperature surfaces that is just above Θ_n or $\theta_{\max}(\theta_{\max} > 1200\,\mathrm{K})$. We note that $\theta_{\min}(\lambda, \phi, t)$ is defined as the minimum value of $\theta(\lambda, \phi, \sigma, t)$, which is always equal to the surface potential temperature except when there exists a superadiabatic layer near the surface in which the mass in the superadiabatic layer is placed in the layer above $\theta_{\min}(\lambda, \phi, t)$. The 15 preselected isentropic surfaces are 260, 270, 280, 290, 300, 315, 330, 350, 370, 400, 450, 550, 650, 850, and 1200 K. The layer between $\theta_{\min}(\lambda, \phi, t)$ and 260 K is labeled as the 250-K layer. The zonal-integrated mass $[m]$ is obtained by integrating the isentropic air mass along each latitude belt.

Similarly, the meridional mass flux and the vertical mass flux due to diabatic heating/cooling between two adjacent sigma surfaces in each grid cube are respectively $v\delta m$ and $\dot\theta\delta m$, where $\dot\theta$ represents the total diabatic heating, which is calculated from 3D temperature, wind, and vertical motion fields. The meridional mass flux F_{ad} between two adjacent isentropic surfaces and the mass-weighted mean diabatic mass flux F_d across each isentropic surface are derived as follows:

$$F_{\mathrm{ad}}(\lambda,\phi,\Theta_n,t) = \int_0^1 [\delta m_\sigma(\lambda,\phi,t)v(\lambda,\phi,\sigma,t)]Y[\theta(\lambda,\phi,\sigma,t),\Theta_n,\Theta_{n+1}]\,d\sigma, \tag{3}$$

$$F_d(\lambda,\phi,\Theta_n,t) = \int_0^1 [\delta m_\sigma(\lambda,\phi,t)\dot\theta(\lambda,\phi,\sigma,t)]Y[\theta(\lambda,\phi,\sigma,t),\Theta_{n-1/2},\Theta_{n+1/2}]\,d\sigma, \tag{4}$$

where $\Theta_{n-1/2}$ is defined as the half isentropic level between Θ_{n-1} and Θ_n. Then we integrated adiabatic and diabatic mass fluxes along each latitude belt and obtained the zonal-integrated adiabatic and diabatic mass flux fields, respectively denoted $[F_{\mathrm{ad}}]$ and $[F_d]$. After that, we calculated the daily mass tendency $(\partial[m]/\partial t)$, divergence of adiabatic mass fluxes $\nabla_\theta[F_{\mathrm{ad}}]$, and divergence of diabatic mass fluxes $(\partial[F_d]/\partial\theta)$ and applied the method of Lagrangian multiplier according to Shin (2012) to obtain a self-consistent mass budget on daily basis that approximately meets the following constraints:

$$\left(\frac{\partial[m]}{\partial t} + \nabla_\theta[F_{\mathrm{ad}}] + \frac{\partial[F_d]}{\partial\theta}\right)_{\phi,\Theta_n,t} = 0, \tag{5}$$

$$\left(\int_{\phi=-\pi}^{\pi} \nabla_\theta[F_{\mathrm{ad}}]\,d\phi\right)_{\Theta_n,t} = 0, \tag{6}$$

$$\left(\int_{\Theta_n=250\,\mathrm{K}}^{1200\,\mathrm{K}} \frac{\partial[F_d]}{\partial\theta}\,d\theta\right)_{\phi,t} = 0. \tag{7}$$

Equation (5) requires that the mass tendency in isentropic tube along latitude is equal to the adiabatic and diabatic mass flux convergence. Equation (6) requires no net mass loss or gain due to adiabatic mass transport in an isentropic layer globally whereas Eq. (7) is the condition that no diabatic mass flux into an atmospheric column from the surface and from the top of the atmosphere. After adjustment, the imbalance of Eq. (5) is reduced to be about 1/10 of the absolute value of the mass tendency in isentropic tube, and residuals of Eqs. (6) and (7) are reduced to be several orders of magnitude smaller than before adjustment.

Obviously, positive (negative) vertical mass fluxes indicate upward (downward) mass fluxes across the isentropic surface, while positive (negative) meridional mass fluxes stand for poleward (equatorward) mass fluxes between two adjacent isentropic surfaces in the Northern Hemisphere. Combining the vertical and the meridional mass flux fields, we obtained the latitude–vertical distribution of isentropic meridional mass circulation. We also calculated the mass streamfunction by

TABLE 1. The year-to-year variance/covariance (10^{30} kg^2) of yearly DJF-mean mass anomalies of the troposphere (below 315 K), the stratosphere (above 315 K), and the total column over the Arctic region (60°–90°N).

Variance	Troposphere	Stratosphere	Total column
Troposphere	3.88	−3.87	0.98
Stratosphere	−3.87	4.84	

summing [F_{ad}] from the top to an isentropic surface, measuring the total air mass transport crossing a latitude circle above that isentropic surface. Positive (negative) values represent a clockwise (anticlockwise) circulation.

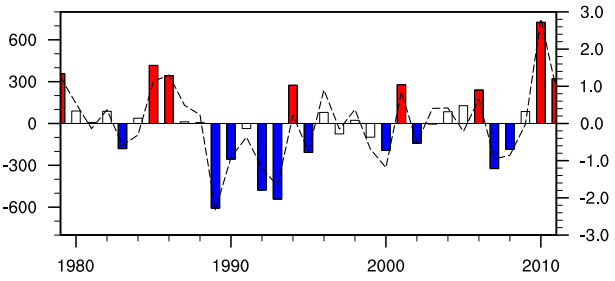

FIG. 1. Year-to-year variations of the DJF-mean Arctic (60°–90°N) Ps anomalies (Pa). Red bars indicate Ps anomalies above 0.5 standard deviations and blue bars represent Ps anomalies below −0.5 standard deviations. Dashed line denotes the yearly variations of AO index derived from DJF-mean geopotential height at 1000 hPa in the domain 20°–90°N.

3. Vertical structure of mass anomalies associated with interannual variability of polar Ps

The climatological-mean potential temperature near the thermal tropopause (Reichler et al. 2003) over the Arctic winter (DJF) is about 307 K. Based on that, we consider the polar air mass in isentropic layers below 315 K as the tropospheric air mass, and that above 315 K as the stratospheric air mass. On average, the DJF-mean column mass over the winter polar cap is about 32.5×10^{16} kg, and more than 70% (24×10^{16} kg) of it resides in the troposphere (below 315 K). However, the year-to-year variance of DJF-mean stratospheric mass (4.84×10^{30} kg^2) is slightly larger than that (3.88×10^{30} kg^2) of tropospheric mass, as shown in Table 1. This implies that interannual changes in the stratospheric mass could play an important role in the interannual variability of total column mass or Ps in the Arctic winter, although tropospheric mass accounts for most of the column mass. It is noteworthy that the air mass in the troposphere and in the stratosphere over the Arctic region has a large negative year-to-year covariance (-3.87×10^{30} kg^2), indicating a large cancellation of air mass anomalies between the two layers. Such out-of-phase relation between mass changes in the stratosphere and that in the troposphere also implies that one of them is positively correlated with the yearly variation of Arctic Ps in winter and the other is negatively correlated.

Year-to-year variations of winter-mean polar Ps anomalies exhibit a noticeable interdecadal variability with positive anomalies dominant in 1979–88 and 2001–11 and negative anomalies in 1989–2000, but without any significant linear trend during the period of 1979–2011 (Fig. 1). The yearly standard deviation of the polar Ps anomalies is about 2.83 hPa. The dashed curve in Fig. 1 is the DJF-mean AO index defined as the standardized principal component of EOF1 of DJF-mean geopotential height anomalies at 1000 hPa over the domain 20°–90°N in the period of 1979–2011 derived from the ERA-Interim dataset. The interannual variations of winter-mean AO index coincide well with polar Ps anomalies with a statistically significant correlation of 0.947, suggesting that polar Ps anomalies discussed in this paper represent the interannual variability of the winter AO.

We applied regression analysis to delineate mass contributions to interannual variations of winter-mean polar Ps anomalies from individual layers. The main features seen from the regressions of isentropic mass anomalies over the Arctic region against polar Ps anomalies (Fig. 2) are (i) mass anomalies in the middle and upper stratosphere (i.e., above 350 K) and in the upper troposphere (between 290 and 315 K) have significant positive correlations with polar Ps anomalies; (ii) mass anomalies in the lower and middle troposphere (i.e., 260–290 K) have significant negative correlations; (iii) mass anomalies in the lower stratosphere (between 315 and 350 K) have very weak correlation; and (iv) mass anomalies near the surface (i.e., below 260 K) have large positive, although not statistically significant, correlations. To confirm the linear regression results in Fig. 2, we show in Fig. 3a the composite means of isentropic mass anomalies for the years when polar Ps anomalies are above 0.5 standard deviations (i.e., red bars in Fig. 1), and in Fig. 3b for the years below −0.5 standard deviations (i.e., blue bars in Fig. 1). The patterns in Figs. 3a and 3b are almost opposite, both confirming the regression results shown in Fig. 2. It is worthwhile to point out that the much smaller values of the composite-mean mass anomalies in layers from 315 to 350 K shown in Fig. 3 do not imply a weaker mass variability in that layer but merely the lack of correlations between the mass anomalies in this layer and the DJF-mean polar Ps anomalies.

According to the regression and composite analyses, we divide the polar column mass into four layers: the

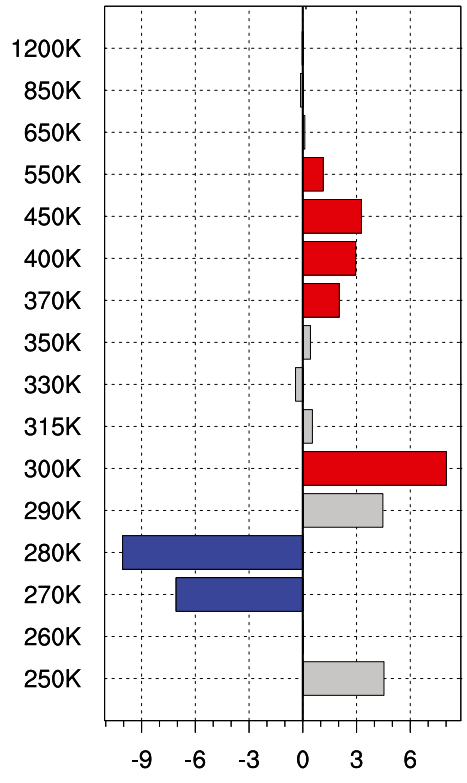

FIG. 2. Linear regressions of the DJF-mean isentropic mass anomalies (10^{14} kg) over the Arctic (60°–90°N) against yearly DJF-mean polar Ps anomalies. Bars in blue and red indicate regressions exceeding 90% confidence level.

layers above 315 K, between 290 and 315 K, between 260 and 290 K, and below 260 K, loosely representing, respectively, the stratospheric layer, the upper tropospheric layer, the lower and middle tropospheric layer, and the surface layer. Plotted in Fig. 4 are scatter diagrams of normalized mass anomalies in each of the four layers (ordinate) against normalized polar Ps anomalies (abscissa). The linear regression lines shown in Fig. 4 indicate that the main features in the vertical structure of mass anomalies remain unchanged after dividing them into four layers. Among the 18 years when polar Ps anomalies are above 0.5 standard deviations or below −0.5 standard deviations, there are 11 years when mass anomalies in the layer above 315 K have an in-phase contribution to Ps anomalies (red points in Fig. 4a). The probability of the in-phase contribution from the 290–315-K layer (red points in Fig. 4b) during large-amplitude events is slightly higher, 12 out of 18 years, although in 2 of the 12 years (1983 and 1985) the in-phase contribution is quite weak. The highest probability (15/18) is found for the out-of-phase contribution to polar Ps anomalies from the 260–290-K layer in years when the amplitude of polar Ps anomalies exceeds 0.5 standard deviations (blue points in Fig. 4c). In the surface layer (Fig. 4d) where the in-phase relation is not statistically significant, the probability of the in-phase relation during large-amplitude events is only 9 out of 18 years.

Figure 4 also suggests that the condition of in-phase contribution from mass anomalies in layers both above 315 K and 290–315 K as well as out-of-phase contribution from mass anomalies in 260–290 K only happens in 7 out of the 18 years of large-amplitude events of polar Ps anomalies. The condition of in-phase contributions from 290–315 K together with out-of-phase contributions from 260–290 K is found in 10 out of the 18 years. However, the condition of coexistence of in-phase contributions from above 315 K and out-of-phase contributions from 260–290 K occurs in most years (14 out of the 18 years). This suggests that the out-of-phase relation between mass anomalies in the stratosphere and those in the middle and lower troposphere is more robust.

4. Interannual variability of winter meridional mass circulation

In the previous section, we have attributed interannual variations of winter-mean polar Ps anomalies to mass anomalies in individual layers. After all, polar Ps anomalies are ultimately caused by net mass anomalies transported into the polar region while mass anomalies in individual layers are determined by the variability in both meridional mass transport and mass exchanges between layers due to diabatic processes. In this section, we examine the interannual variability of the meridional mass circulation in winter and quantitatively account its contributions to polar Ps anomalies and the vertical pattern of mass anomalies.[1]

a. Interannual variations of the winter-mean meridional mass circulation

The isentropic meridional mass circulation has been documented using daily data (e.g., Johnson 1989; Cai and Shin 2014) and climatological monthly-mean meridional mass fluxes (Czaja and Marshall 2006; Pauluis et al. 2008, 2010) on dry and moist isentropes. Here we

[1] The residual circulation analysis does not provide quantitative information on mass accumulation or depletion in an atmospheric column due to meridional mass transport because the residual circulation is nondivergent by definition, although one can qualitatively relate the residual circulation intensity variation to the annular mode variability as well as polar Ps anomalies [see Haynes (2005), and references therein].

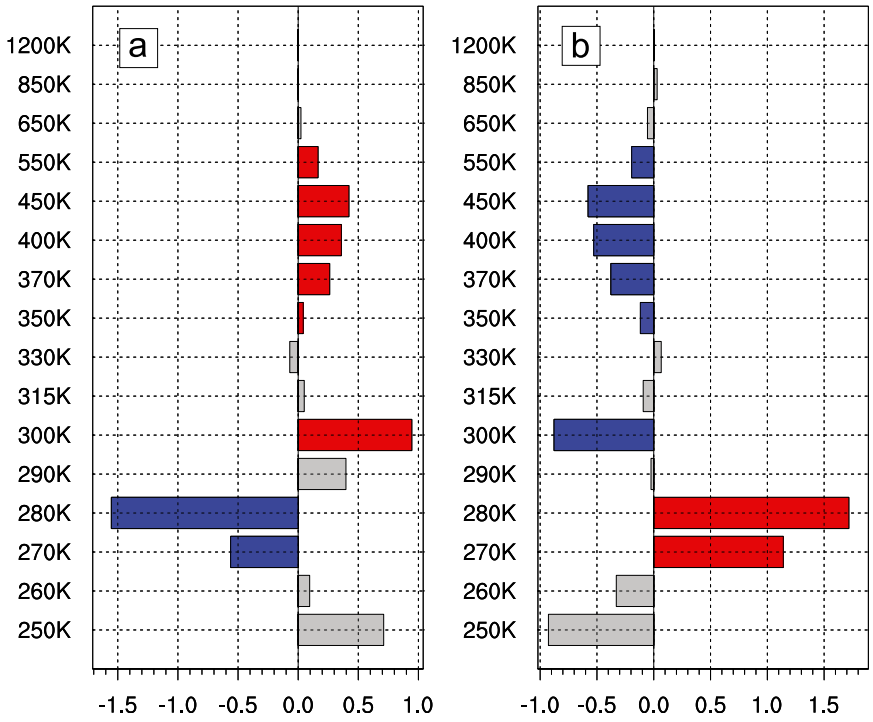

FIG. 3. Composite means of DJF-mean isentropic mass anomalies (10^{15} kg) over the Arctic for years (a) when Ps anomalies are above 0.5 standard deviations and (b) when Ps anomalies are below −0.5 standard deviations. Bars in blue and red indicate composites exceeding 90% confidence level.

derived the daily-mean fields of mass streamfunction and zonal-integrated adiabatic and diabatic mass fluxes extended to higher isentropic surface (up to 1200 K) from 1979 to 2011 using the ERA-Interim dataset. Similar to the previous studies, the winter (DJF) climatological-mean fields (Fig. 5) show a meridional overturning mass circulation consisting of a poleward branch (or warm branch) in upper layers and an equatorward branch (or cold branch) in lower layers and diabatic upward mass fluxes in the tropics and downward fluxes in high latitudes. Embedded in the hemispheric cell are three subcells, representing the tropical Hadley cell, a thermally direct circulation in the extratropical troposphere [which is referred to as the extratropical Hadley cell (EHC) in Cai and Shin (2014)], and the Brewer–Dobson circulation (BDC) in the stratosphere (Dobson et al. 1929; Brewer 1949).

Linear regressions of DJF-mean mass streamfunction anomalies (Fig. 6a) against the DJF-mean polar Ps anomalies suggest that the interannual variability of DJF-mean polar Ps and the intensity of meridional mass circulation in the extratropics are positively correlated, as indicated by a hemispheric anomalous clockwise circulation above 350 K and an anomalous clockwise circulation in the extratropics below 350 K with larger values in winters when polar Ps anomalies are positive. Specifically, the significantly positive meridional mass flux anomalies over the extratropics in layers between 350 and 450 K and layers between 290 and 330 K in (Fig. 6b) indicate the strengthening of the poleward branch. Weak mass flux anomalies around 330 K coincide well with small values of climatological-mean mass fluxes in this layer (Fig. 5b), which seems to be the boundary between the poleward branch of the BDC and that of the EHC. The stronger poleward mass transport into the polar cap is accompanied with a stronger downward mass transport via diabatic cooling processes (Fig. 6c), bringing more air from the polar stratosphere and upper troposphere to the lower troposphere below. The strengthened mass fluxes into the lower troposphere feed a strengthening of the equatorward branch in the lower troposphere (Fig. 6b), transporting more mass out of the Arctic region. In short, among winters with positive polar Ps anomalies, meridional mass flux anomalies into the polar region are mostly positive above 315 K, positive in 290–315 K, and negative in 260–290 K, respectively indicating the intensified poleward branch of the BDC, poleward branch of the EHC, and equatorward

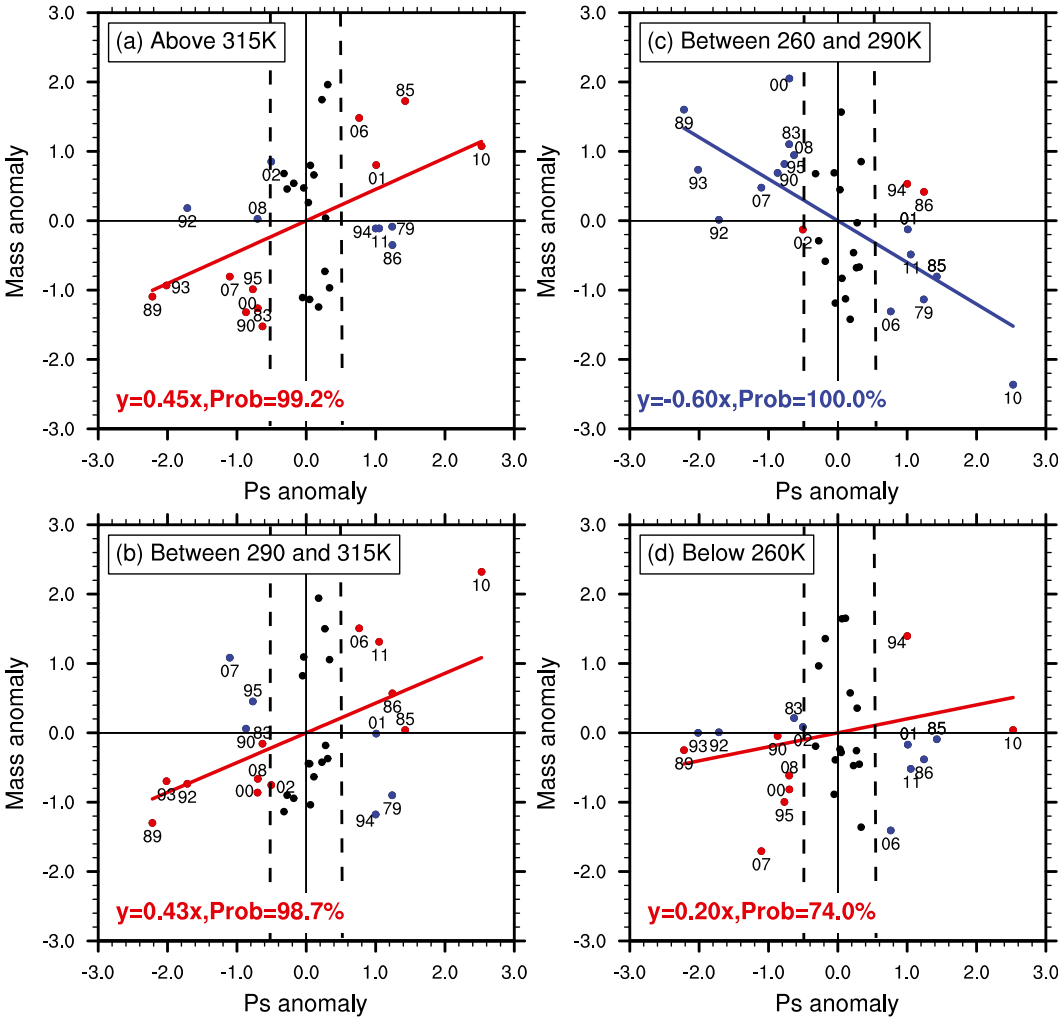

FIG. 4. Scatterplots of normalized DJF-mean Ps anomalies (abscissa) and mass anomalies (ordinate) (a) above 315 K, (b) between 290 and 315 K, (c) between 260 and 290 K, and (d) below 260 K over the Arctic. Ps anomalies exceeding ±0.5 standard deviations are marked with their years of occurrence. Thick color lines are the linear regression lines corresponding to the linear regression equations and confidence level shown in the left bottom of each plot. Red (blue) dots represent in-phase (out of phase) mass anomalies with Ps anomalies.

branch in lower levels. This is consistent with the vertical structure of mass anomalies associated with polar Ps anomalies reported in the previous section, and the more robust out-of-phase relation of mass anomalies between the layer above 315 K and that at 260–290 K found in the previous section seemingly implies a more robust relation between yearly variations of the stratospheric poleward branch and the equatorward branch in the lower troposphere in winter.

b. *Attribution of winter-mean polar Ps anomalies to interannual variations of timing and intensity of mass transport into and out of the polar region*

According to the previous section, the meridional mass circulation is significantly intensified (weakened) in the extratropics in winters with positive (negative) winter-mean polar Ps anomalies as evident from simultaneous intensifications of the poleward branch in upper layers, diabatic downward mass transport, and the equatorward branch in lower layers. Next, we will conduct a mass budget analysis over the winter polar region to quantitatively examine how interannual variations of winter-mean polar Ps anomalies are related to interannual variations of the meridional mass circulation in the extratropics in winter seasons. Note that the winter mean of mass transport anomalies into the polar atmospheric column is directly related to the winter-mean tendency of polar Ps anomalies, instead of winter-mean Ps anomalies. To account for winter-mean Ps anomalies, we need to know the temporal distribution

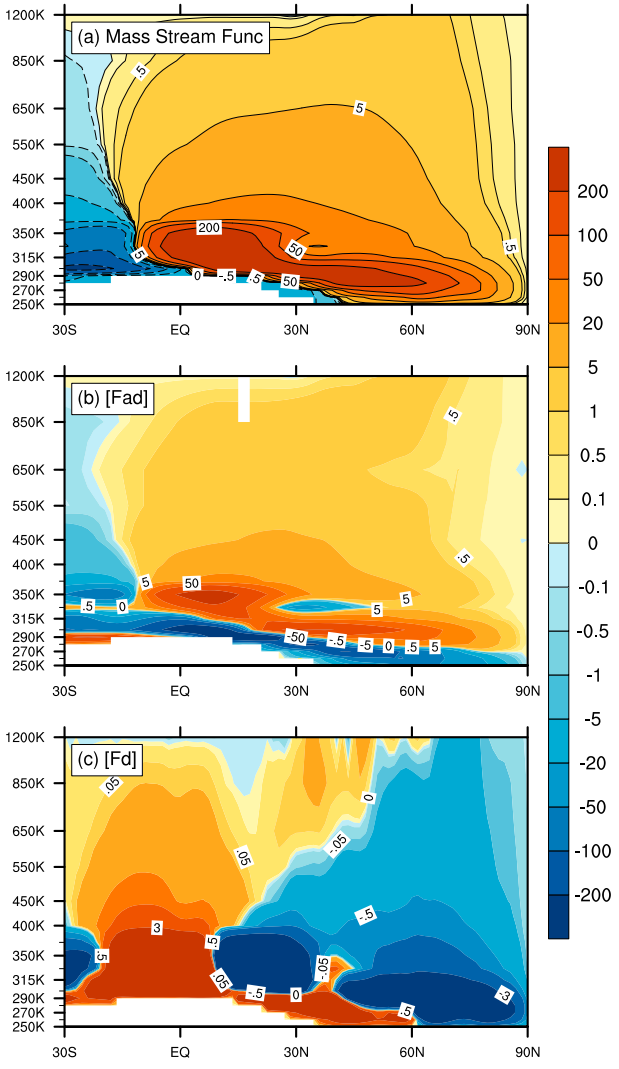

FIG. 5. The DJF-mean climatology of (a) mass streamfunction ($10^9\,\mathrm{kg\,s^{-1}}$), (b) zonal-integrated meridional/adiabatic mass fluxes ($10^9\,\mathrm{kg\,s^{-1}}$), and (c) zonal-integrated vertical/diabatic mass fluxes ($10^9\,\mathrm{kg\,s^{-1}}$).

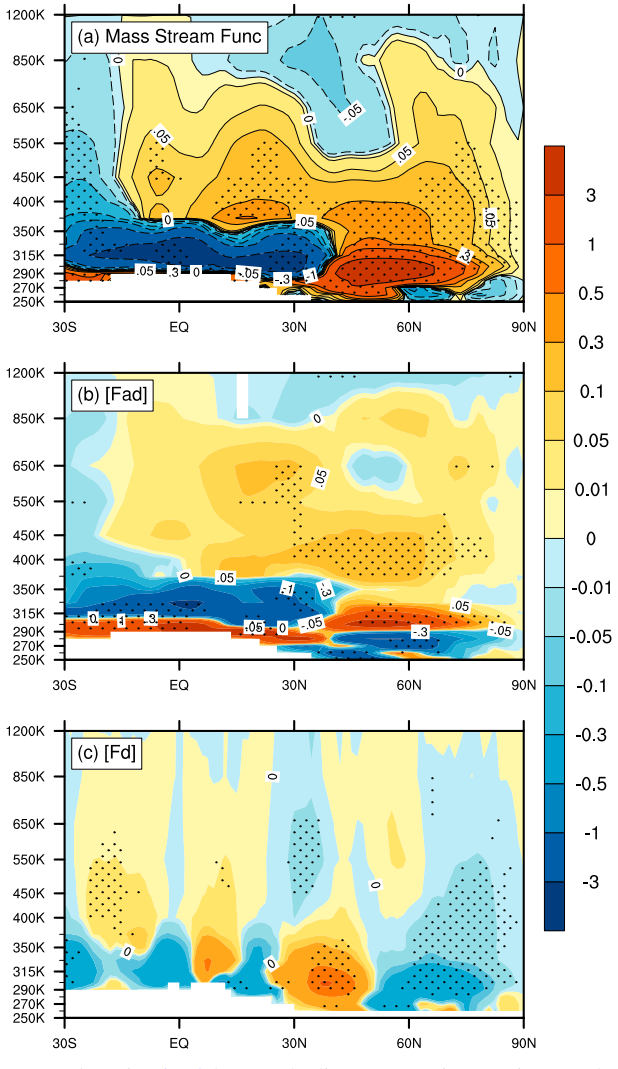

FIG. 6. As in Fig. 5, but for the linear regressions against yearly DJF-mean Arctic Ps anomalies. Dotted areas indicate regressions exceeding 90% confidence level.

of daily mass transport anomalies into and out of the polar region in the winter season and the total-column mass anomalies at the beginning day of the winter. For winter-mean mass anomalies in individual layers, the temporal distribution of daily mass anomalies into and out of individual layers diabatically is also needed, even though it does not contribute to surface pressure anomalies.

To evaluate contributions to winter-mean polar Ps anomalies from circulation anomalies in individual layers, our mass budget analysis is conducted for the four layers aforementioned, namely above 315, 290–315, 260–290, and below 260 K, representing the poleward branch in the stratosphere and upper troposphere, the equatorward branch in the lower troposphere, and the layer near the surface. Based on the mass budget equation, the mass anomaly over the polar region at time t in layer k (one of the four layers), denoted $M'(k, t)$, is determined from

$$M'(k,t) = M'(k,t_0) + \int_{t_0}^{t} [A'_M(k,\tau) + D'_M(k,\tau)]\, d\tau, \tag{8}$$

where $M'(k, t_0)$ is the mass anomaly at t_0 ($t_0 < t$) in the same layer k over the polar region and $\int_{t_0}^{t} [A'_M(k, \tau) + D'_M(k, \tau)]\, d\tau$ is the anomalous mass brought into the layer k over the polar region from t_0 to t by adiabatic $[A'_M(k, \tau)]$ and diabatic $[D'_M(k, \tau)]$ processes. The mass anomaly averaging over a period from t_0 to t_N is

$$\frac{1}{t_N - t_0}\int_{t_0}^{t_N} M'(k,t)\,dt = M'(k,t_0) + \frac{1}{t_N - t_0}\int_{t_0}^{t_N}\left\{\int_{t_0}^{t}\left[A'_M(k,\tau) + D'_M(k,\tau)\right]d\tau\right\}dt. \quad (9)$$

Applying Eq. (9) to daily data (i.e., $dt = d\tau = 1$ day), we have

$$\frac{1}{N}\sum_{n=1}^{N} M'(k,t_n) = M'(k,t_0) + \frac{1}{N}\sum_{n=1}^{N}\sum_{j=1}^{n}\left[A'_M(k,t_j) + D'_M(k,t_j)\right]. \quad (10)$$

For the DJF mean, t_0 corresponds to 30 November and t_N corresponds to 28 February, and $N = 90$. The monthly contributions to the DJF-mean polar layer mass anomalies are

$$\overline{M'(k)}^{\mathrm{DJF}} = M'(k,\text{Nov. }30) + T_A^{\mathrm{Dec}}(k) + T_D^{\mathrm{Dec}}(k) + T_A^{\mathrm{Jan}}(k) + T_D^{\mathrm{Jan}}(k) + T_A^{\mathrm{Feb}}(k) + T_D^{\mathrm{Feb}}(k), \quad (11)$$

where

$$T_A^{\mathrm{Dec}}(k) = \sum_{n=1}^{31}\frac{91-n}{90}A'_M(k,t_n), \quad T_D^{\mathrm{Dec}}(k) = \sum_{n=1}^{31}\frac{91-n}{90}D'_M(k,t_n),$$

$$T_A^{\mathrm{Jan}}(k) = \sum_{n=32}^{62}\frac{91-n}{90}A'_M(k,t_n), \quad T_D^{\mathrm{Jan}}(k) = \sum_{n=32}^{62}\frac{91-n}{90}D'_M(k,t_n),$$

$$T_A^{\mathrm{Feb}}(k) = \sum_{n=63}^{90}\frac{91-n}{90}A'_M(k,t_n), \quad T_D^{\mathrm{Feb}}(k) = \sum_{n=63}^{90}\frac{91-n}{90}D'_M(k,t_n), \quad (12)$$

where $T_A^{\mathrm{Dec}}(k) + T_D^{\mathrm{Dec}}(k)$, $T_A^{\mathrm{Jan}}(k) + T_D^{\mathrm{Jan}}(k)$, and $T_A^{\mathrm{Feb}}(k) + T_D^{\mathrm{Feb}}(k)$ correspond to contributions to the DJF-mean mass anomaly from the net anomalous mass brought to the layer k by adiabatic transport (with the subscript A) and diabatic transport (with the subscript D) in the months of December, January, and February, respectively.

Displayed in Fig. 7 are the results obtained from Eq. (11) after applying regression against DJF-mean polar Ps anomalies. In winters when winter-mean polar Ps anomalies are positive, more mass is brought into the polar region in the layers above 290 K by the poleward branch and more mass is brought out in the layers below 290 K by the equatorward branch from December to February and vice versa. In winters with positive (negative) winter-mean polar Ps anomalies, the peak of the strengthening (weakening) of the stratospheric poleward branch (above 315 K) occurs in December, 1 month earlier than the peak of the strengthening (weakening) of the poleward branch in the upper troposphere (290–315 K) and the equatorward branch in the lower troposphere (260–290 K). Contributions from anomalous mass changes due to diabatic processes tend to be out of phase with adiabatic contributions in all layers. The net contribution to the DJF-mean mass anomalies in the layer above 315 K over the polar cap is dominated by the adiabatic component in December but these two processes tend to totally offset in January and February. Therefore, the positive winter-mean mass anomalies above 315 K (0.95×10^{15} kg) in a winter of positive polar Ps anomalies are mostly (91.6%) due to anomalous mass transported by the poleward mass circulation into the polar stratosphere in December. The anomalies (6.19×10^{15} kg) due to cross-isentropic mass transport from upper layers to the 290–315-K layer in winter by diabatic cooling in the stratosphere contribute positively to mass anomalies in layers below. The strengthening of the poleward mass transport in the 290–315-K layer also contributes mass anomalies there positively. The sum of the mass influx anomalies from these two components exceeds anomalous mass brought down to the layer below via diabatic cooling in December and January, which is responsible for the positive correlation between winter-mean mass anomalies in the 290–315-K layer and winter-mean polar Ps anomalies. Mass anomalies brought out of the polar region by the companion equatorward mass transport in the 260–290-K layer is greater than mass anomalies brought down via diabatic cooling from the poleward branch in December and January. This, together with the upwelling of the lower isentropic surface (i.e., downward mass transport crossing the 260-K surface via diabatic cooling) in December, contributes to the negative mass anomalies in the 260–290-K layer associated with positive winter-

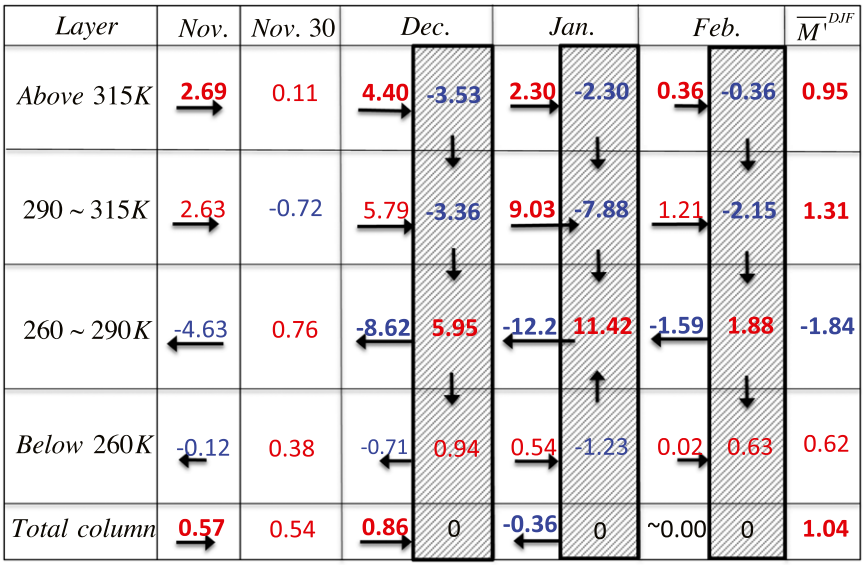

FIG. 7. Regressions of contributions to (column 6) yearly DJF-mean mass anomalies from mass anomalies on (column 2) 30 November, and mass anomalies brought by meridional or adiabatic mass flux (numbers above horizontal arrows) and cross-isentropic or diabatic mass flux (numbers inside hatched boxes) in individual layers above the Arctic in the months of (column 3) December, (column 4) January, and (column 5) February. (column 1) The regressed contributions by meridional mass flux in November. (bottom) The vertical sum of all layers or the total column above the Arctic. Units are 10^{15} kg and numerals are red for positive values and blue for negative values. Boldface numbers indicate regressions exceeding the 90% confidence level. Right- (left-) pointing arrows represent the meridional mass transport into (out of) the Arctic region, and upward and downward arrows indicate the direction of the cross-isentropic mass transport at each interface between two adjacent isentropic layers.

mean polar Ps anomalies. Anomalous mass changes associated with elevation changes of the lower isentropic surface, as indicated by positive mass anomalies transported from the 260–290-K layer in December and February, account for the positive correlation in the layer next to the surface in early winter, although it is not statistically significant.

The DJF-mean total-column mass anomaly over the polar region (or polar Ps anomalies) is attributed from mass anomalies transported into and/or out of the polar region in the total column. The vertical summation of Eq. (11) over all layers yields

$$\sum_k \overline{M'(k)}^{\mathrm{DJF}} = \sum_k M'(k, \text{Nov. } 30) + \sum_k T_A^{\mathrm{Dec}}(k) + \sum_k T_A^{\mathrm{Jan}}(k) + \sum_k T_A^{\mathrm{Feb}}(k). \quad (13)$$

The regression of DJF-mean total-column mass anomalies over the polar region obtained from Eq. (13) against DJF-mean polar Ps anomalies is 1.041×10^{15} kg (or about 2.85 hPa in terms of mean Ps anomaly) as shown in Fig. 7, very close to the standard deviation of interannual variability of the DJF-mean polar Ps anomalies (1.03×10^{15} kg or 2.83 hPa). About 48% (0.501×10^{15} kg) of the DJF-mean total-column mass anomalies, on average, is brought into the polar column by anomalous meridional mass circulation in DJF and the remaining 52% (0.54×10^{15} kg) corresponds to the total mass anomalies that have been inside the polar region before December begins (30 November). Mass anomalies on 30 November equal the sum of total mass anomalies transported in during November (0.57×10^{15} kg, indicated in the leftmost column in Fig. 7) and the small column mass anomaly on 31 October (-0.03×10^{15} kg). In November and December, mass anomalies transported into the polar column by the poleward branch are greater than mass anomalies transported out by the equatorward branch, contributing 1.43×10^{15} kg to positive polar Ps anomalies in the DJF mean. It is noteworthy that mass anomalies transported in by the stratospheric poleward branch are nearly as large as those by the poleward branch in the upper troposphere despite the fact that more mass resides in the upper troposphere than in the stratosphere. This again suggests that besides the contribution from the anomalous

poleward branch in the upper troposphere to the interannual variability of winter-mean polar Ps anomalies, the contribution from the anomalous poleward branch in the stratosphere is also important. In January when the year-to-year variability of the meridional circulation in the extratropical troposphere is strongest, mass anomalies transported out by the equatorward branch become greater than mass anomalies transported in by the poleward branch, contributing negatively to polar Ps anomalies in DJF. In February, mass anomalies transported out by the equatorward branch are nearly as large as those transported in by the poleward branch, contributing little to polar Ps anomalies in DJF. Therefore, DJF-mean polar Ps anomalies are mainly contributed from anomalous mass transport into the upper polar region by the poleward branch above 290 K in earlier winter months from November to December. The polar mass accumulation in November and December and the polar mass depletion in January seem to suggest that the strengthening or weakening of the poleward branch in the upper levels leads that of the equatorward branch in lower levels.

5. Interannual variability of wave activities in the extratropics

Planetary wave activities in the stratosphere play an important role in the stratosphere–troposphere coupling by affecting the tropospheric circulations (e.g., Holton et al. 1995; Kuroda and Kodera 1999; Hartley et al. 1998; Ambaum and Hoskins 2002; Black 2002). As mentioned in the introduction, the meridional mass circulation in the extratropics is driven by baroclinically amplifying waves [referred to as the geostrophic component of the meridional mass transport in Townsend and Johnson (1985) and Johnson (1989)], in contrast with that in the tropics, which is driven mainly by the ageostrophic component with little presence of waves. Therefore, it is expected that there would be presence of large-amplitude waves when the meridional mass circulation over the polar region is stronger and vice versa.

In the previous section, we presented the evidence indicating that the stronger meridional mass circulation in winter extratropics leads to positive winter-mean polar Ps anomalies and vice versa. In this section, we wish to link the interannual variability of meridional mass circulation to anomalous wave amplitudes in the extratropical stratosphere in winter seasons. Following Zhang et al. (2013), we calculated the wave amplitude index (WAI) from the total geopotential height fields z (without removing the climatological annual cycle) at each latitude ϕ, pressure level p, and time t according to

$$\mathrm{WAI}(\phi, p, t) = \sqrt{\overline{[z(\lambda,\phi,p,t) - \overline{z(\lambda,\phi,p,t)}^{\lambda}]^2}^{\lambda}}, \qquad (14)$$

where the overbar with superscript λ denotes the zonal mean operator over the entire latitude circle at the latitude ϕ. The anomaly field of WAI is obtained by removing its climatological annual cycle. Positive anomalies of WAI represent higher zonal asymmetry of the geopotential height field or larger wave amplitude, and vice versa.

Figure 8 shows regressions of monthly-mean anomalies of WAI at 100, 50, 20, 10, and 1 hPa in months from September to March against DJF-mean polar Ps anomalies. It is seen that in a winter when DJF-mean polar Ps anomalies are positive (negative), anomalous large (small) amplitude of waves emerges as early as October and continues to grow (weaken) in November and December. This is in a good agreement with the timing of strengthening (weakening) of meridional mass circulation in extratropics as shown in Figs. 6 and 7. Figure 8 also shows that WAI anomalies appear to originate first from midlatitudes and propagate poleward. Meanwhile WAI anomalies at upper levels tend to reach the Arctic earlier than those at lower levels, exhibiting a poleward and downward propagation. This is in accordance with the poleward- and downward-propagating signals in the convergence of anomalous Eliassen–Palm (E-P) flux (e.g., Kuroda and Kodera 1999).

Since variations of wave activities in the stratosphere are mainly from wavenumbers 1 and 2, we have obtained the WAI of wavenumbers 1 and 2 by substituting the total geopotential height z in Eq. (9) with components of wavenumbers 1 and 2, respectively. Regressions of monthly-mean WAI anomalies of these two dominant wave components (Figs. 9 and 10) against the DJF-mean polar Ps anomalies show that WAI anomalies of wavenumbers 1 and 2 in the stratosphere are both positively correlated with winter-mean polar Ps anomalies. WAI anomalies of wavenumber 1 associated with polar Ps anomalies are 3 times as large as those of wavenumber 2 and make a dominant contribution to WAI anomalies of total wave activities.

6. Concluding remarks

We have quantitatively examined the interannual variability of surface pressure (Ps) over the Arctic in winter seasons and its attributions from the meridional mass circulation variability using the ERA-Interim data from 1979 to 2011. Results show that the interannual variability of winter-mean polar Ps is positively correlated

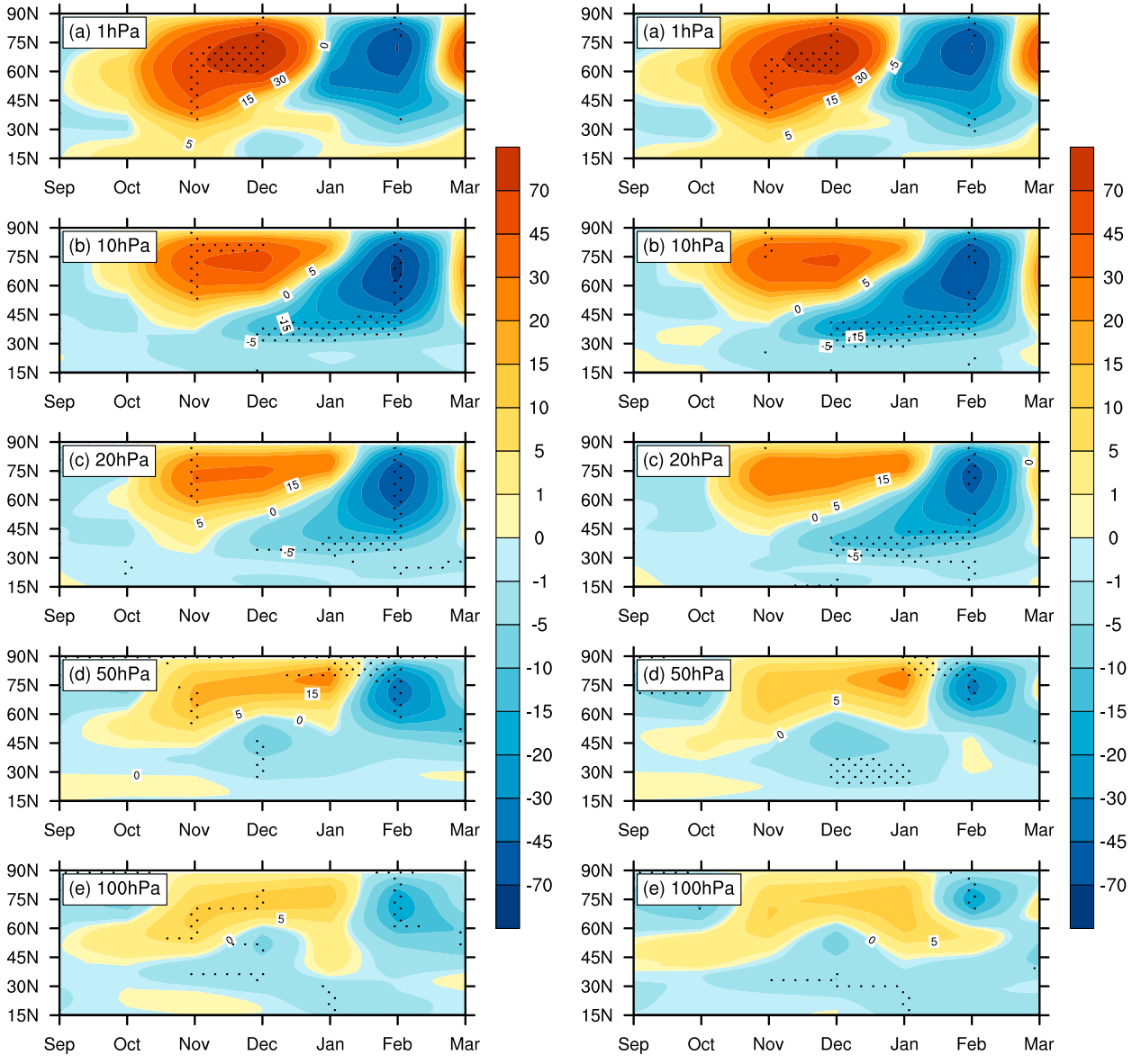

FIG. 8. Latitude–time cross-sectional diagrams of regressed monthly-mean anomalies of WAI (m) from September to March at (a) 1, (b) 10, (c) 20, (d) 50, and (e) 100 hPa against yearly DJF-mean Arctic Ps anomalies. Dotted areas indicate regressions exceeding 90% confidence level.

FIG. 9. As in Fig. 8, but for wavenumber 1.

with air mass changes in upper troposphere and stratosphere (above 290 K) but negatively correlated with those in the middle and lower troposphere (260–290 K). It is also positively correlated with air mass changes near the surface (below 260 K), but the correlation is not as significant as that for the layers above. Such vertical structure of layer mass anomalies associated with polar Ps anomalies explains why mass changes in the polar stratosphere contribute greatly to the year-to-year variability of the winter polar Ps, as indicated by the slightly larger year-to-year variability of the winter stratospheric air mass (above 315 K) compared with the winter tropospheric air mass.

The interannual variability of polar Ps in winter is intimately related to the interannual variability of meridional mass circulation in the extratropics. Regressions of winter-mean adiabatic and diabatic mass fluxes against polar Ps anomalies show significant intensification of meridional mass circulation in the extratropics associated with positive polar Ps anomalies as evident from simultaneously intensifications of the poleward branch in upper layers, the diabatic downward mass transport, and the equatorward branch in lower

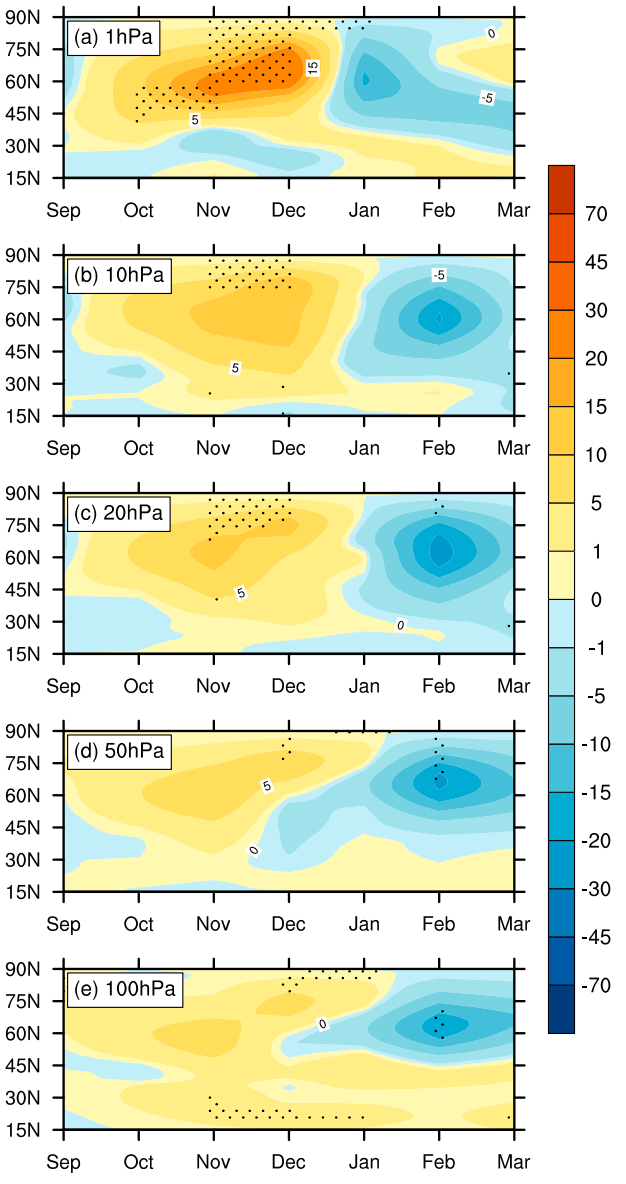

FIG. 10. As in Fig. 8, but for wavenumber 2.

layers. Our mass budget analysis reveals that higher winter-mean polar Ps are mainly attributed to the anomalous mass brought into the polar region by the poleward branch in upper layers, which overwhelms the anomalous mass transported out in lower layers by the equatorward branch in earlier winter months November and December. In January, mass anomalies transported out by the equatorward branch become greater than mass anomalies transported in by the poleward branch, contributing negatively to polar Ps anomalies in DJF. For DJF-mean mass anomalies in each isentropic layer, contributions from the anomalous mass brought into and/or out of the polar region tend to be partly canceled by mass changes due to anomalous diabatic cooling, but the sign of the net mass contribution in individual layers is determined by the meridional mass transport in most cases during December and January when the net mass changes contribute positively to DJF-mean mass anomalies associated with polar Ps anomalies.

Although such mass budget attribution does not necessarily lead to a causal relationship, it provides quantitative attribution of interannual variations of winter-mean polar Ps anomalies and layer mass anomalies to the intensity and timing of anomalous mass transport by the meridional mass circulation in winter. This also helps to gain a better understanding of the coupling mechanism of stratospheric mass–temperature anomalies and the surface pressure–temperature anomalies via variability of the global meridional mass circulation. In the upper atmosphere, anomalous mass brought by poleward warm-air branch tends to exceed the anomalous mass brought down by diabatic cooling, leading to positive mass anomalies in upper levels when the meridional circulation is stronger or to negative mass anomalies for a weaker meridional mass circulation. This corresponds to an anomalous warm high in the upper polar atmosphere when polar Ps anomalies are positive (Fig. 11). Meanwhile, a higher winter-mean polar Ps, which is due to more mass transported into the polar column by a stronger poleward branch than mass transported out in earlier winter, tends to accompany negative polar temperature anomalies at lower levels, although they are not statistically significant (Fig. 11). It follows that at interannual time scales, the polar atmosphere also exhibits a seemingly equivalent barotropic structure, namely a warm high anomaly in the upper atmosphere above a cold high anomaly at the surface or cold low anomaly in the upper atmosphere above a warm high anomaly at the surface, as in the case of intraseasonal variability (e.g., Cai and Ren 2007).

Our study also shows that the interannual variability of the meridional mass circulation intensity in winter seasons coincides well with that of planetary wave activities (particularly both wavenumbers 1 and 2) in the extratropics. This establishes that it is year-to-year variations of wave activities that drive year-to-year variations of meridional mass circulation in the extratropics, contributing to year-to-year variations of winter-mean polar Ps anomalies. Many studies have demonstrated that the variability of wave activities in the extratropical stratosphere, variations of polar night jet, and variability of polar Ps are all interrelated (e.g., Hartmann 1983; Baldwin et al. 2007; Kuroda and Kodera 2004). It is expected that the interannual variability of meridional mass circulation should also link to interannual variations of polar night jet via its companion momentum transport and pressure torque, which needs to be explored in future work.

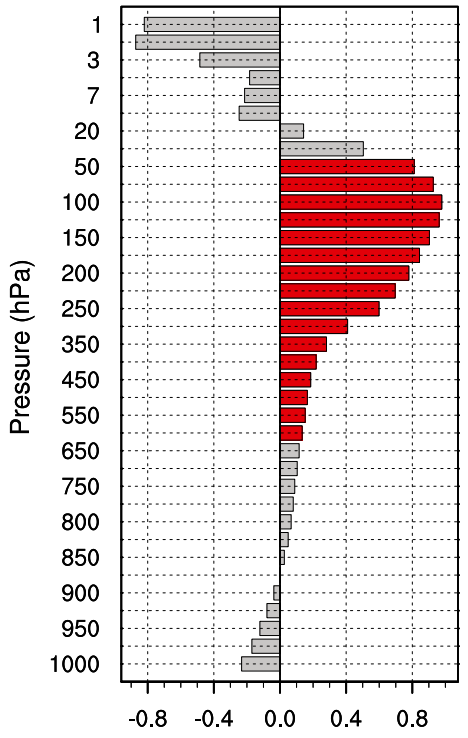

FIG. 11. Regressions of DJF-mean temperature anomalies averaging over the Arctic region against yearly DJF-mean Arctic Ps anomalies. Bars in red and blue indicate regressions exceeding the 90% confidence level.

Acknowledgments. This work was supported by the National Basic Research Program of China 2010CB428603. The authors are grateful to the three anonymous reviewers for their constructive and insightful comments that greatly helped to improve the presentation.

REFERENCES

Ambaum, M. H. P., and B. J. Hoskins, 2002: The NAO troposphere–stratosphere connection. *J. Climate,* **15,** 1969–1978, doi:10.1175/1520-0442(2002)015<1969:TNTSC>2.0.CO;2.

Baldwin, M. P., 2001: Annular modes in global daily surface pressure. *Geophys. Res. Lett.,* **28,** 4115–4118, doi:10.1029/2001GL013564.

——, and T. J. Dunkerton, 1999: Propagation of the Arctic Oscillation from the stratosphere to the troposphere. *J. Geophys. Res.,* **104,** 30 937–30 946, doi:10.1029/1999JD900445.

——, and ——, 2001: Stratospheric harbingers of anomalous weather regimes. *Science,* **294,** 581–584, doi:10.1126/science.1063315.

——, P. B. Rhines, H.-P. Huang, and M. E. McIntyre, 2007: Atmospheres: The jet-stream conundrum. *Science,* **315,** 467–468, doi:10.1126/science.1131375.

Balling, R. C., Jr., and M. P. Lawson, 1982: Twentieth century changes in winter climatic regions. *Climatic Change,* **4,** 57–69, doi:10.1007/BF02423313.

Black, R. X., 2002: Stratospheric forcing of surface climate in the Arctic Oscillation. *J. Climate,* **15,** 268–277, doi:10.1175/1520-0442(2002)015<0268:SFOSCI>2.0.CO;2.

Brewer, A. W., 1949: Evidence for a world circulation provided by the measurements of helium and water vapour distribution in the stratosphere. *Quart. J. Roy. Meteor. Soc.,* **75,** 351–363, doi:10.1002/qj.49707532603.

Cai, M., and R.-C. Ren, 2007: Meridional and downward propagation of atmospheric circulation anomalies. Part I: Northern Hemisphere cold season variability. *J. Atmos. Sci.,* **64,** 1880–1901, doi:10.1175/JAS3922.1.

——, and C.-S. Shin, 2014: A total flow perspective of atmospheric mass and angular momentum circulations: Boreal winter mean state. *J. Atmos. Sci.,* **71,** 2244–2263, doi:10.1175/JAS-D-13-0175.1.

Charney, J. G., and P. G. Drazin, 1961: Propagation of planetary-scale disturbances from the lower into the upper atmosphere. *J. Geophys. Res.,* **66,** 83–109, doi:10.1029/JZ066i001p00083.

Czaja, A., and J. Marshall, 2006: The partitioning of poleward heat transport between the atmosphere and ocean. *J. Atmos. Sci.,* **63,** 1498–1511, doi:10.1175/JAS3695.1.

Dee, D. P., and Coauthors, 2011: The ERA-Interim reanalysis: Configuration and performance of the data assimilation system. *Quart. J. Roy. Meteor. Soc.,* **137,** 553–597, doi:10.1002/qj.828.

Dobson, G. M. B., D. N. Harrison, and J. Lawrence, 1929: Measurements of the amount of ozone in the earth's atmosphere and its relation to other geophysical conditions. Part III. *Proc. Roy. Soc. London,* **122,** 456–486, doi:10.1098/rspa.1929.0034.

Geller, M. A., and J. C. Alpert, 1980: Planetary wave coupling between the troposphere and the middle atmosphere as a possible sun–weather mechanism. *J. Atmos. Sci.,* **37,** 1197–1214, doi:10.1175/1520-0469(1980)037<1197:PWCBTT>2.0.CO;2.

Gillett, N. P., M. R. Allen, R. E. McDonald, C. A. Senior, D. T. Shindell, and G. A. Schmidt, 2002: How linear is the Arctic Oscillation response to greenhouse gases? *J. Geophys. Res.,* **107,** 4022, doi:10.1029/2001JD000589.

——, F. W. Zwiers, A. J. Weaver, and P. A. Stott, 2003: Detection of human influence on sea-level pressure. *Nature,* **422,** 292–294, doi:10.1038/nature01487.

——, R. J. Allan, and T. J. Ansell, 2005: Detection of external influence on sea level pressure with a multi-model ensemble. *Geophys. Res. Lett.,* **32,** L19714, doi:10.1029/2005GL023640.

Hartley, D. E., J. T. Villarin, R. X. Black, and C. A. Davis, 1998: A new perspective on the dynamical link between the stratosphere and troposphere. *Nature,* **391,** 471–474, doi:10.1038/35112.

Hartmann, D. L., 1983: Barotropic instability of the polar night jet stream. *J. Atmos. Sci.,* **40,** 817–835, doi:10.1175/1520-0469(1983)040<0817:BIOTPN>2.0.CO;2.

Haynes, P., 2005: Stratospheric dynamics. *Annu. Rev. Fluid Mech.,* **37,** 263–293, doi:10.1146/annurev.fluid.37.061903.175710.

Hines, C. O., 1974a: A possible mechanism for the production of sun–weather correlations. *J. Atmos. Sci.,* **31,** 589–591, doi:10.1175/1520-0469(1974)031<0589:APMFTP>2.0.CO;2.

——, 1974b: *The Upper Atmosphere in Motion. Geophys. Monogr.,* Vol. 18, Amer. Geophys. Union, 1027 pp.

Holton, J. R., and C. Mass, 1976: Stratospheric vacillation cycles. *J. Atmos. Sci.,* **33,** 2218–2225, doi:10.1175/1520-0469(1976)033<2218:SVC>2.0.CO;2.

——, P. H. Haynes, M. E. McIntyre, A. R. Douglass, R. B. Rood, and L. Pfister, 1995: Stratosphere–troposphere exchange. *Rev. Geophys.,* **33,** 403–439, doi:10.1029/95RG02097.

Johnson, D. R., 1989: The forcing and maintenance of global monsoonal circulations: An isentropic analysis. *Advances in Geophysics,* Vol. 31, Academic Press, 43–316, doi:10.1016/S0065-2687(08)60053-9.

Kodera, K., K. Yamazaki, M. Chiba, and K. Shibata, 1990: Downward propagation of upper stratospheric mean zonal wind perturbation to the troposphere. *Geophys. Res. Lett.,* **17,** 1263–1266, doi:10.1029/GL017i009p01263.

——, M. Chiba, H. Koide, A. Kitoh, and Y. Nikaidou, 1996: Interannual variability of the winter stratosphere and troposphere in the Northern Hemisphere. *J. Meteor. Soc. Japan,* **74,** 365–382.

Kuroda, Y., 2005: On the influence of the meridional circulation and surface pressure change on the Arctic Oscillation. *J. Geophys. Res.,* **110,** D21107, doi:10.1029/2004JD005743.

——, and K. Kodera, 1999: Role of planetary waves in the stratosphere–troposphere coupled variability in the Northern Hemisphere winter. *Geophys. Res. Lett.,* **26,** 2375–2378, doi:10.1029/1999GL900507.

——, and ——, 2004: Role of the polar-night jet oscillation on the formation of the Arctic Oscillation in the Northern Hemisphere winter. *J. Geophys. Res.,* **109,** D11112, doi:10.1029/2003JD004123.

L'Heureux, M. L., and R. W. Higgins, 2008: Boreal winter links between the Madden–Julian oscillation and the Arctic Oscillation. *J. Climate,* **21,** 3040–3050, doi:10.1175/2007JCLI1955.1.

——, A. Butler, B. Jha, A. Kumar, and W. Wang, 2010: Unusual extremes in the negative phase of the Arctic Oscillation during 2009. *Geophys. Res. Lett.,* **37,** L10704, doi:10.1029/2010GL043338.

Limpasuvan, V., D. W. J. Thompson, and D. L. Hartmann, 2004: The life cycle of the Northern Hemisphere sudden stratospheric warmings. *J. Climate,* **17,** 2584–2596, doi:10.1175/1520-0442(2004)017<2584:TLCOTN>2.0.CO;2.

Lorenz, E. N., 1951: Seasonal and irregular variations of the Northern Hemisphere sea-level pressure profile. *J. Meteor.,* **8,** 52–59, doi:10.1175/1520-0469(1951)008<0052:SAIVOT>2.0.CO;2.

Matsuno, T., 1970: Vertical propagation of stationary planetary waves in the winter Northern Hemisphere. *J. Atmos. Sci.,* **27,** 871–883, doi:10.1175/1520-0469(1970)027<0871:VPOSPW>2.0.CO;2.

Miller, A. J., S. Zhou, and S.-K. Yang, 2003: Relationship of the Arctic and Antarctic Oscillations to the outgoing longwave radiation. *J. Climate,* **16,** 1583–1592, doi:10.1175/1520-0442-16.10.1583.

Moritz, R. E., C. M. Bitz, and E. J. Steig, 2002: Dynamics of recent climate change in the Arctic. *Science,* **297,** 1497–1502, doi:10.1126/science.1076522.

Overland, J. E., and M. Wang, 2005: The Arctic climate paradox: The recent decrease of the Arctic Oscillation. *Geophys. Res. Lett.,* **32,** L06701, doi:10.1029/2004GL021752.

Pauluis, O., A. Czaja, and R. Korty, 2008: The global atmospheric circulation on moist isentropes. *Science,* **321,** 1075–1078, doi:10.1126/science.1159649.

——, ——, and ——, 2010: The global atmospheric circulation in moist isentropic coordinates. *J. Climate,* **23,** 3077–3093, doi:10.1175/2009JCLI2789.1.

Perlwitz, J., and N. Harnik, 2003: Observational evidence of a stratospheric influence on the troposphere by planetary wave reflection. *J. Climate,* **16,** 3011–3026, doi:10.1175/1520-0442(2003)016<3011:OEOASI>2.0.CO;2.

Reichler, T., M. Dameris, and R. Sausen, 2003: Determining the tropopause height from gridded data. *Geophys. Res. Lett.,* **30,** 2042, doi:10.1029/2003GL018240.

Ren, R.-C., and M. Cai, 2007: Meridional and vertical out-of-phase relationships of temperature anomalies associated with the northern annular mode variability. *Geophys. Res. Lett.,* **34,** L07704, doi:10.1029/2006GL028729.

——, and ——, 2008: Meridional and downward propagation of atmospheric circulation anomalies. Part II: Southern Hemisphere cold season variability. *J. Atmos. Sci.,* **65,** 2343–2359, doi:10.1175/2007JAS2594.1.

Sato, Y., 1974: Vertical structure of quasi-stationary planetary waves in several winters. *J. Meteor. Soc. Japan,* **52,** 272–282.

Shindell, D. T., R. L. Miller, G. A. Schmidt, and L. Pandolfo, 1999: Simulation of recent northern winter climate trends by greenhouse-gas forcing. *Nature,* **399,** 452–455, doi:10.1038/20905.

Shin, C.-S., 2012: A hybrid Lagrangian/Eulerian view of the global atmospheric mass circulation: Seasonal cycle. Ph.D. dissertation, Florida State University, 144 pp.

Sigmond, M., P. C. Siegmund, and H. Kelder, 2003: Analysis of the coupling between the stratospheric meridional wind and the surface level zonal wind during 1979–93 Northern Hemisphere extratropical winters. *Climate Dyn.,* **21,** 211–219, doi:10.1007/s00382-003-0328-2.

Thompson, D. W. J., and J. M. Wallace, 1998: The Arctic Oscillation signature in the wintertime geopotential height and temperature fields. *Geophys. Res. Lett.,* **25,** 1297–1300, doi:10.1029/98GL00950.

——, and ——, 2001: Regional climate impacts of the Northern Hemisphere annular mode. *Science,* **293,** 85–89, doi:10.1126/science.1058958.

——, M. P. Baldwin, and J. M. Wallace, 2002: Stratospheric connection to Northern Hemisphere wintertime weather: Implications for prediction. *J. Climate,* **15,** 1421–1428, doi:10.1175/1520-0442(2002)015<1421:SCTNHW>2.0.CO;2.

Townsend, R. D., and D. R. Johnson, 1985: A diagnostic study of the isentropic zonally averaged mass circulation during the first GARP global experiment. *J. Atmos. Sci.,* **42,** 1565–1579, doi:10.1175/1520-0469(1985)042<1565:ADSOTI>2.0.CO;2.

Walsh, J. E., W. L. Chapman, and T. L. Shy, 1996: Recent decrease of sea level pressure in the central Arctic. *J. Climate,* **9,** 480–486, doi:10.1175/1520-0442(1996)009<0480:RDOSLP>2.0.CO;2.

Waugh, D. W., W. J. Randel, S. Pawson, P. A. Newman, and E. R. Nash, 1999: Persistence of the lower stratospheric polar vortices. *J. Geophys. Res.,* **104,** 27 191–27 201, doi:10.1029/1999JD900795.

Zhang, Q., C.-S. Shin, H. Van den Dool, and M. Cai, 2013: CFSv2 prediction skill of stratospheric temperature anomalies. *Climate Dyn.,* **41,** 2231–2249, doi:10.1007/s00382-013-1907-5.

Zhou, S., and A. J. Miller, 2005: The interaction of the Madden–Julian oscillation and the Arctic Oscillation. *J. Climate,* **18,** 143–159, doi:10.1175/JCLI3251.1.